Published in final edited form as:
J Phys Chem B. 2008 October 2; 112(39): 12279–12285. doi:10.1021/jp805026m.

Lipid bilayer curvature and pore formation induced by charged linear polymers and dendrimers: the effect of molecular shape

Hwankyu Lee[1,*] and **Ronald G. Larson**[2]

1*Laboratory of Computational Biology, National Heart, Lung, and Blood Institute, National Institutes of Health, Bethesda, MD 20892, USA*

2*Department of Chemical Engineering, Biomedical Engineering, Mechanical Engineering, and Macromolecular Science and Engineering Program, University of Michigan, Ann Arbor, MI 48109, USA*

Abstract

We performed molecular dynamics (MD) simulations of multiple copies of poly-L-lysine (PLL) and charged polyamidoamine (PAMAM) dendrimers in dimyristoylphosphatidylcholine (DMPC) bilayers with explicit water using the coarse-grained model developed by Marrink et al. (*J. Chem. Theory and Comput*. **2008**, 4, 819). Membrane disruption is enhanced at higher concentrations and charge densities of both spheroidally shaped dendrimers and linear PLL polymers, in qualitatively agreement with experimental studies by Hong et al. (*Bioconjugate Chem*. **2006**, 17, 728). However, larger molecular size enhances membrane disruption and pore formation only for dendrimers and not for the linear PLL. Despite more intimate electrostatic interactions of linear molecules than are possible for spheroidal dendrimers, only the dendrimers were found to perforate membranes, apparently because they cannot spread onto a single leaflet, and so must penetrate the bilayer to get favorable electrostatic interactions with head groups on the opposite leaflet. These results indicate that a relatively rigid spheroidal shape is more efficient than a flexible linear shape in increasing membrane permeability. These results compare favorably with experimental findings.

INTRODUCTION

Because the targeting of nanoparticles and polymers to cell membranes shows promise for biomedical applications, such as antitumor therapeutics and drug delivery,[1-5] the interactions between membranes and nanoparticles have been widely studied.[6-18] Polyamidoamine (PAMAM) dendrimers are among the best candidates due to their controlled mass, water solubility, and surface functionality.[19,20] The interactions of these with membranes have been studied, for example, by the group of Banaszak Holl, Orr, Baker, and coworkers, using *in vitro* enzyme assays and atomic force microscopy (AFM). These studies have shown that charged G5 and G7 dendrimers can, respectively, expand existing holes, and initiate hole formation in lipid bilayers.[21-23] They found that dendrimer size, concentration, and terminal-acetylation significantly affect pore formation in lipid bilayers, effects that were confirmed by our previous molecular dynamics (MD) simulations[24,25] and by the mesoscale thermodynamic modeling of Ginzburg and Balijepalli.[13]

The interactions of membranes with cationic polymers such as linear poly-L-lysine (PLL), branched polyethylenimine (PEI), and ring-containing diethylaminoethyl-dextran (DEAE-DEX) were studied experimentally by Hong et al.[26] Although in these studies the hydrodynamic radius of the PEI used was smaller than that of DEAE-DEX, the PEI polymer

*Corresponding author (email: leeh3@nhlbi.nih.gov)

induced greater membrane permeability than did DEAE-DEX, apparently due to the high charge density of the former. These results suggested that polymer size does not affect membrane permeabilization as much as charge density does.[26] However, although the linear molecule PLL also has an order of magnitude higher charge/monomer ratio than does either the ring-shaped DEAE-DEX or charged spheroidal G5 dendrimers, Hong et al. showed that all three of these molecules, at similar concentrations, produced similar levels of enzyme leakage out of cells, polymer internalization into cells, and transport of small dye molecules into and out of cells.[26] These results suggest that, for a given charge/monomer ratio, spheroidal molecules or nanoparticles may be more efficient at increasing membrane permeability than are linear polymers. More recently, however, Leroueil et al.[11] found that cationic polymers and nanoparticles with higher surface areas induce more nanoparticle-lipid disruption.[11] This finding seems to conflict with the above-mentioned results of Hong et al.[26] that indicated little effect of polymer size on membrane permeability. This might be because in Leroueil et al.[11] surface areas were compared for molecules of different shapes (linear, branched, ring-containing, and spheroidal), rather than comparing molecules of the same shape but different size. For example, they found that a short linear peptide (MSI-78), with a relatively low surface area, disrupts membranes more weakly than do large spherical or branched molecules with larger surface areas. Thus, the relative effects of size and shape (or surface area) cannot be determined from these studies alone. Apparently conflicting experimental results might be resolved by considering separately the effects of polymer size and shape on pore formation. It is quite possible that pore formation is controlled not by any single factor, but by a combination of charge density, size, concentration, and shape.

To investigate this, we here describe coarse-grained (CG) MD simulations of the interaction of PLL with a dimyristoylphosphatidylcholine (DMPC) bilayer and compare these results with those for spheroidal dendrimeric molecules. Results for PLL were obtained from new simulations reported here, while those for dendrimers were obtained by extending previous 160 ns simulations of un-acetylated (charged) G5 and G7 dendrimers in DMPC bilayers out to 240 ns. We compare membrane curvature and electrostatic interactions of PLL with those for dendrimers as a function of charge density, size, and concentration. The results are rationalized in terms of the effect of shape anisotropy on membrane curvature.

METHODS

All simulations and analyses were performed with the GROMACS3.3.2 simulation package[27] with the "MARTINI" CG force field developed by Marrink et al.,[28,29] which we downloaded from http://md.chem.rug.nl/~marrink/coarsegrain.html. A cutoff of 12 Å was used for van der Waals interactions. With use of the standard shift function of GROMACS[27] in which both the energy and force vanish at the cutoff distance, the LJ potential was smoothly shifted to zero between 0.9 and 1.2 nm to reduce the cutoff noise. Although electrostatic interactions in the CG MARTINI force field are ordinarily parameterized by using a cutoff of 12 Å with a shift function, our previous work showed that long-range electrostatics needs to be included to simulate pore formation induced by dendrimers. Fortunately, we showed that inclusion of long-range electrostatic interactions does not significantly change the area per lipid and lateral diffusion coefficients in a CG DMPC bilayer.[25] (The areas per lipid had been matched to experimental values through optimization of the CG LJ parameters in the absence of long-range electrostatics,[28,30] and so large changes in area/lipid produced by inclusion of electrostatic interactions would have necessitated re-optimizing the LJ parameters.) Therefore, electrostatic interactions were modeled using a combination of a short-range electrostatic interaction with a cutoff of 12 Å and particle mesh Ewald summation (PME).[31]

The temperature was maintained at 310 K by applying a Berendsen thermostat in the NPT ensemble.[32] A time step of 20 fs was used, and the coordinates were saved every 20 ps for analysis. Note that because of the smoothing of the potentials in the CG model, diffusive motion is faster than in atomistic simulations and so the effective time sampled in CG simulations is 3-6 times larger than in atomistic simulations, and hence the effective simulation time step is approximately 80 fs. Hereafter all simulation times reported in this paper are effective times, which are taken to be four times longer than the normal simulation time.

Equilibration of a CG poly-L-lysine

Atomic coordinates of 128, 146, and 256-residue poly-L-lysine (respectively, called PLL128, PLL146, and PLL256) were generated using Swiss-Pdb Viewer.[33] Atomic coordinates were converted to the CG coordinates, and topologies of the CG PLL model were generated for the coil structure using scripts available from the same website above. In brief, for lysine monomers, within MARTINI, a CG lysine consists of a polar bead, an apolar bead, and a charged bead, which respectively represent backbone, side chain carbon, and side chain amino groups. Backbone beads of the CG PLL are connected by a weak harmonic potential $V_{bond}(R)$ with an equilibrium distance $R_{bond} = 0.350$ nm ($V_{bond}(R) = \frac{1}{2}K_{bond}(R - R_{bond})^2$, where K_{bond} = 200 kJ mol^{-1} nm^{-2}), and a weak harmonic angle potential with an equilibrium angle θ_0 = 127° ($V_{angle}(\theta) = \frac{1}{2}K_{angle}\{\cos(\theta) - \cos(\theta_0)\}^2$, where K_{angle} = 25 kJ mol^{-1}). For interactions between a backbone bead and a side chain bead, R_{bond} = 0.330 nm, K_{bond} = 5000 kJ mol^{-1} nm^{-2}, θ_0 = 100° (backbone-backbone-side chain), and K_{angle} = 25 kJ mol^{-1} were used. For interactions between side chain beads, R_{bond} = 0.280 nm, K_{bond} = 5000 kJ mol^{-1} nm^{-2}, θ_0 = 180° (backbone-side chain-side chain), and K_{angle} = 25 kJ mol^{-1} were used.

To model PLL as a random coil, appropriate harmonic bonding and angle potential energy functions (but, no dihedrals) were used, which are also already parameterized for peptides with random coil structure within MARTINI. Each PLL was simulated for 500 ns in explicit CG water with enough counterions (128, 146, and 256 Cl^- for PLL128, PLL146, and PLL256, respectively) to achieve electroneutrality, and the last 180 ns of the trajectory was used for analysis.

Equilibration of poly-L-lysine with a DMPC bilayer

The final configurations of PLL molecules simulated in water were used as the initial configurations of the PLL-bilayer system. Multiple copies (four, eight, and 16 for PLL128; four for PLL256) of the equilibrated PLL128 and PLL256 were added to the bilayer systems equilibrated in our previous work.[25] The center of mass of each PLL was positioned a distance of 5-6 nm above the center of bilayer. The final system included multiple PLL molecules, 8192 DMPC molecules, ~290000 CG waters (which is equivalent to ~1160000 real waters), and enough counterions (512, 1024, or 2048 Cl^-) to neutralize the system in a box of size 50 × 50 × 18 nm^3 (Table 1 and Figure 1). After several steps of energy minimization, PLL and the bilayer were positioned-restrained with a force constant of 1000 kJ mol^{-1} nm^{-2}, and an equilibration run of 400 ps was performed. After the restrained equilibration, an unrestrained equilibration run was performed for 200 ns, and the last 40 ns of the trajectory was used for analysis. In addition to simulations of PLL in DMPC bilayers, simulations of the G5 or G7 dendrimer-bilayer systems, which in our previous work[25] had been simulated for 160 ns and showed bilayer deformation or hole formation, were extended up to 240 ns under the same simulation conditions as earlier (Table 1). Parameterization and verification of the CG dendrimer model were described in our previous work.[24,25]

RESULTS AND DISCUSSION

Simulations of a coarse-grained PLL

To verify our CG model for PLL, root-mean-squared end-to-end distances were calculated and compared with values from experiments. Experimentally, Brant and Flory obtained a characteristic ratio, C_∞, of 8.6 ± 0.9 for PLL in aqueous 1M NaBr (θ condition).[34] Here, $C_\infty = \langle R^2 \rangle_0 / n_p l_p^2$, where $\langle R^2 \rangle_0$ is the mean square unperturbed distance between the polymer chain ends, n_p is the degree of polymerization, and l_p is the fixed distance of 3.80 Å between the α-carbons of the *trans* peptide repeating units in the chain. In good solvents, due to the excluded volume effect, the linear dimensions of a PLL coil of molecular weight 115,000 Daltons exceed by a factor of 1.33 the theta dimension.[34] This swelling effect, present in good solvents, is a well-known phenomenon in polymer solutions and can be modeled using the Flory expression for the so-called swelling coefficient α, which is the ratio of the radius of gyration in a good solvent to that of a polymer of the same length in a theta solvent. A theta solvent is a solvent in which the chain takes on a random walk configuration, i.e., in which there is no swelling. The Flory expression is : $\alpha^5 - \alpha^3 = \frac{4}{3} z = KN^{1/2}$,[35] where K is a constant and N is the number of residues. Using the factor of 1.33 expansion for a molecular weight 115,000 chain, we can obtain the constant K, and then compute the swelling coefficient for any chain length. Thus, we obtain the root-mean-square end-to-end distances of PLL128, PLL146, and PLL256 of, respectively, 154 ± 15, 166 ± 17, and 226 ± 23 Å. In Figure 2, our simulations show that end-to-end distances fluctuate but otherwise do not change systematically after 320 ns, and their autocorrelation functions yield decay times below 50 ns, indicating that PLL are equilibrated within the simulated time scales. In Table 2, root-mean-square end-to-end distances calculated from our simulations PLL128, PLL146, and PLL256 are respectively 162 ± 49, 159 ± 53, and 296 ± 47 Å, which are in agreement within the error bars with the above predictions based on experimental data, indicating that our CG PLL models successfully represent the random coil structure of PLL.

The effect of polymer size and concentration on bilayer curvature and pore formation

Multiple copies of the equilibrated PLL128 and PLL256 were simulated near a DMPC bilayer for 200 ns. These PLL-bilayer systems are named “PLL128-4”, “PLL128-8”, “PLL128-16”, and “PLL256-4”, where the first and second numbers describe the number of lysine residues per PLL and the number of PLL molecules, respectively (Table 1). To compare the behaviors of these linear molecules with those of spheroidal ones, we also extended the G5 and G7 dendrimer-bilayer systems up to 240 ns. In our previous work, membrane curvature or pore formation was observed only in the systems including one or four charged G7 dendrimers, or 16 charged G5 dendrimers, whereas charged dendrimers at lower concentration and neutral dendrimers did not cause pore formation or membrane curvature.[25] Here, we extend simulations that showed membrane curvature or pore formation, namely “G5-16”, “G7-1”, and “G7-4”, where the first and second number describe the dendrimer generation and number of dendrimers, respectively.

Figure 1 shows snapshots from the beginning (*left* and *middle image*) and end of all the simulations (*right image*). Final configurations show that the bilayer is deformed for PLL128-8 and PLL128-16, but not for PLL128-4, indicating that PLL concentration affects membrane curvature, which was also observed in the dendrimer-bilayer systems of our previous work.[25] Figure 3 shows that radii of gyration averaged over PLL molecules in each system change at the beginning of the simulations, but do not change much over the rest of the simulation time, indicating that the PLL molecules in the bilayers have at least reached a local equilibrium within the simulated time scale. In the extended dendrimer-bilayer simulations, the membrane curvature and pore formation observed within the first 160 ns remain relatively unchanged

over the extended 80 ns. Figure 4 shows the time dependence of the bilayer height, defined as the maximum distance between glycerols of DMPC along the direction of the bilayer normal. In G7-4, the bilayer height drastically increases with time after the beginning of the simulation and then reaches an apparent steady-state value at around 180 ns. A rapid increase in the bilayer height was also observed in G7-1 and G5-16; however for G5-16, the bilayer height eventually decreases and reaches a much lower value at around 180 ns, indicating that at high concentrations the smaller dendrimers ultimately induce less bilayer curvature at steady state than do the larger ones. Also, for G7-1 the bilayer height eventually decreases to a value almost as low as that for G5-16 at 240 ns, indicating that a sufficiently high dendrimer concentration is important for deforming the bilayer.

For the systems shown in Figure 4, the bilayer height of PLL128-8 is much greater than that of PLL128-4, consistent with the concentration effect that we found in the G7 dendrimer systems. The bilayer heights of PLL128-4 and PLL256-4 were the same to within statistical error, indicating that the size of linear polymers has much less effect on membrane curvature than does that of spheroidal dendrimers. For PLL-bilayer systems, pore formation was not observed even in PLL128-16, which has the highest concentration of PLL molecules. Note that PLL128-16 and G5-16 have the same number of positive charges per molecule as well, and G5-16 showed pore formation in our previous work.[25] However, PLL molecules in PLL128-16 did not insert into the bilayer at any time during the simulation, indicating that insertion of PLL cannot be captured even at this high concentration. To see if PLL-induced pore formation can be observed in small bilayer systems (PLL:lipid ratio of 1:512), we simulated a single PLL128 and a single G5 dendrimer in a small 512-DMPC bilayer for 400 ns. Note that G5-16 (16 G5 dendrimers with 8192 lipids) has dendrimer:lipid ratio of 1:512, and showed pore formation in our previous work.[25] Consistent with this, a single G5 dendrimer inserted into the 512-DMPC bilayer in our previous work.[24] However, a single PLL128 did not insert into the small 512-lipid bilayer, consistent with the simulation of PLL128-16 in a large 8192-lipid system, since they have the same ratio of 1:512, confirming again that insertion of PLL cannot be observed at this high concentration. In Figure 5, the bilayer tails in G5-16, PLL128-4, PLL128-8, PLL128-16, and PLL256-4 are more disordered than in the pure bilayer, and those in PLL128-8 and PLL128-16 are more disordered than in G5-16, PLL128-4, and PLL256-4. This indicates that although no pore formation occurred in PLL128-8 and PLL128-16 over our simulation time scale, leakage or even pore formation could well eventually occur in both of these systems, as is observed in experiments.[26]

Difference in the charge interactions resulting from different molecular shapes

In addition to size and concentration, it has been shown in many experimental studies[21,22] that the charge of nanoparticles or polymers is important for pore formation. Our previous work showed that electrostatic interactions between anionic phosphate groups of the bilayer and cationic terminals of the dendrimer play an important role in pore formation.[25] To compare the electrostatic effects of PLL and dendrimers, we computed the radial distribution functions (RDF's) of DMPC phosphate groups of all lipids of both leaflets of the bilayer around the side chains of PLL in PLL128-8, and around terminals of the dendrimer that had inserted or had adsorbed but remained un-inserted into the bilayer in G5-16. In Figure 6, although PLL128 and the G5 dendrimer have the same number of positive charges per molecule, the RDF for the side chains of PLL128 has a much higher peak at ~0.5 nm than does that of terminals of the un-inserted dendrimers. From the cumulative RDF, we find that there are around 0.27 phosphates in the first coordination shell (<5.1Å) for the side chains of PLL128, while there are around 0.14 phosphates for terminals of the un-inserted G5 dendrimers, indicating that PLL128 has stronger electrostatic interactions with lipid headgroups than does the G5 dendrimer. This is expected, since most charged residues of linear polymers are accessible to the lipid headgroups, which is not the case for the charged terminals of a spheroidal dendrimer.

Thus, linear polymers can have stronger electrostatic interactions with a bilayer than can spheroidal dendrimers. Despite this, pore formation was observed in G5-16, but not in PLL128-8. Interestingly, the RDF value for the inserted dendrimers is very close to that for PLL128, which is much higher than that for the un-inserted dendrimers. This result can be explained by noting that since a dendrimer cannot spread onto a single leaflet like PLL can, a dendrimer has to penetrate the bilayer to have strong favorable electrostatic interactions with head groups on the opposite leaflet, and so achieve comparable numbers of such interactions as PLL already has on a single leaflet. These results indicate that linear structures show a weaker tendency for pore formation because they can interact stably with a single leaflet.

The effect of molecular shape on membrane permeability

As discussed above, the weaker size effect of PLL, the smaller membrane curvature, and absence of pore formation, despite the stronger electrostatic interactions of PLL, might be explained by the difference in shape between the linear and spheroidal polymers. To quantify the effect of the molecular shape on the bilayer curvature, we computed the aspect ratios, I_z/I_x and I_z/I_y, where I_z, I_y, and I_x are principal moments of inertia, ordered such that $I_z > I_y > I_x$, and obtained from these the relative shape anisotropy, κ^2 ($\kappa^2 = 1 - 3I_2/I_1^2$, where I_1 and I_2 are the first and second invariants of the radius of gyration tensor ($I_1 = I_x + I_y + I_z$, $I_2 = I_x I_y + I_y I_z + I_x I_z$)). A linear array of skeletal atoms is characterized by $\kappa^2 = 1$, while a molecule with tetrahedral or higher symmetry is characterized by $\kappa^2 = 0$.[36] We previously computed those values for G5 dendrimers, and the aspect ratios, I_z/I_y and I_z/I_x, were 1.2~1.3 and 1.2~1.5, and relative shape anisotropies were 0.01, indicating that dendrimers are spheroidal with modestly ellipsoidal shape.[37] When interacting with bilayers, this spherical shape of dendrimers is still retained throughout the entire simulation.

Table 3 shows that I_z/I_y and I_z/I_x of PLL128 are 1.1 and 7.3, respectively, and the κ^2 value is 0.16, indicating that, not surprisingly, PLL is much more planar than are dendrimers. The I_z/I_x and κ^2 values of PLL256 (14.5 and 0.20, respectively) are higher than for PLL128, showing that PLL256 is more anisotropic than PLL128. When interacting with bilayers (PLL128-4, PLL128-8, and PLL256-4), those values vary from one PLL molecule to the next. However, the aspect ratios and anisotropies of some PLL molecules in PLL128-8 are much lower than for PLL256-4, and all molecules in PLL256-4 retain their high aspect ratios and anisotropies. The higher aspect ratio of PLL in PLL256-4 may impede membrane curvature, although the total number of charges in PLL256-4 is same as those in PLL128-8. These results indicate that spheroidal polymers increase the bilayer curvature more than linear ones do. Note that although for PLL128-4 each molecule has a relatively low aspect ratio and anisotropy, the bilayer does not bend, while membrane curvature is prominent in PLL128-8, showing again the effect of concentration on the membrane curvature.

Experimentally, by measuring enzyme leakage induced by DEAE-DEX, PEI, PLL, and charged G5 dendrimers, Hong et al. showed that PEI, which has the greatest charge density, induces much more membrane permeability than do DEAE-DEX, PLL, or G5 dendrimers, although the hydrodynamic radius of the DEAE-DEX studied (M_w=608321) is larger than that of the PEI (M_w=269077).[26] Therefore, Hong et al. suggested that (1) the size of the polymer does not seem to markedly affect its ability to induce membrane permeability, and (2) charge interactions are important for membrane permeability. However, although PLL has an order of magnitude higher charge per unit molecular mass than do DEAE-DEX and charged G5 dendrimers, the observed difference in enzyme leakage induced by these molecules was not remarkable, suggesting that (3) spheroidal (dendrimers), branched (PEI), or ring-containing (DEAE-DEX) structures are more effective, for a given charge density, than are linear polymers (PLL) in increasing membrane permeability. Our previous work[25] showed that larger dendrimers induce more membrane curvature and pore formation than do smaller ones, in

agreement with experimental studies.[21-23] However, in our simulations of PLL interacting with the bilayer, a larger PLL size does not increase membrane curvature or pore formation, in agreement with experimental observations by Hong et al.,[26] as described above. These results suggest that the size of spheroidal polymers can significantly affect membrane curvature and pore formation, but the size of linear polymers cannot. However, for both PLL and dendrimers, we found that a higher concentration induces greater membrane curvature or, for dendrimers, pore formation, which agrees with experimental observations,[26] suggesting that high concentration is an important factor regardless of the polymer shape. We previously showed that charged dendrimers can insert into the bilayer, but neutral dendrimers cannot, again in agreement with experimental studies.[21] Also, strong electrostatic interactions between cationic terminals of the dendrimer and anionic phosphate groups of the bilayer were found to be very important for pore formation. However, in the PLL-bilayer systems having differently sized PLL but the same total charges (PLL128-8 and PLL256-4), membrane curvature was observed only in the system with less anisotropic PLL polymers (PLL128-8), suggesting that the shape of charged polymers is a key factor controlling membrane curvature and permeability.

CONCLUSIONS

Coarse-grained molecular dynamics simulations of multiple copies of poly-L-lysine (PLL) and charged polyamidoamine (PAMAM) dendrimers in a DMPC bilayer were performed to investigate the effects of molecular shape on membrane curvature and pore formation. Our simulation results indicate that cationic polymer or dendrimer-induced membrane disruption and pore formation are influenced by multiple properties of the polymers or dendrimers. Higher charge density and concentration induce more membrane disruption for both linear PLL and spheroidal shaped dendrimers, in qualitatively agreement with experimental studies.[21-23, 26] However, we find that larger size leads to more disruption for spheroidal polymers, but not for linear ones. Also, although the flexible linear polymer PLL has more intimate electrostatic interactions with the head groups of the bilayer, rigid spheroidal polymers induce more membrane curvature and pore formation because they cannot exhaust their favorable electrostatic interactions through attachment to a single leaflet, while flexible linear polymers can. These results suggest that a relatively rigid spheroidal shape is more efficient than a flexible linear shape in increasing membrane permeability. This seems to be in agreement with experiments.

ACKNOWLEDGMENT

This research was supported by the Intramural Research Program of the National Institutes of Health, National Heart, Lung, and Blood Institute. This study utilized the high-performance computational capabilities of the CIT Biowulf/ LoBoS3 and NHLBI LOBOS clusters at the National Institutes of Health, Bethesda, MD.

References

1. Popielarski SR, Pun SH, Davis ME. Bioconjugate Chemistry 2005;16:1063. [PubMed: 16173781]
2. Segura T, Shea LD. Annual Review of Materials Research 2001;31:25.
3. Davis ME. Current Opinion in Biotechnology 2002;13:128. [PubMed: 11950563]
4. Ferrari M. Nature Reviews Cancer 2005;5:161.
5. Rolland AP. Critical Reviews in Therapeutic Drug Carrier Systems 1998;15:143. [PubMed: 9592627]
6. Nel A, Xia T, Madler L, Li N. Science 2006;311:622. [PubMed: 16456071]
7. Leroueil PR, Hong SY, Mecke A, Baker JR, Orr BG, Holl MMB. Accounts of Chemical Research 2007;40:335. [PubMed: 17474708]
8. Zhang LF, Granick S. Nano Letters 2006;6:694. [PubMed: 16608266]
9. El-Sayed IH, Huang XH, El-Sayed MA. Nano Letters 2005;5:829. [PubMed: 15884879]

10. Roiter Y, Ornatska M, Rammohan AR, Balakrishnan J, Heine DR, Minko S. Nano Letters 2008;8:941. [PubMed: 18254602]
11. Leroueil PR, Berry SA, Duthie K, Han G, Rotello VM, McNerny DQ, Baker JR, Orr BG, Holl MMB. Nano Letters 2008;8:420. [PubMed: 18217783]
12. Fischlechner M, Reibetanz U, Zaulig M, Enderlein D, Romanova J, Leporatti S, Moya S, Donath E. Nano Letters 2007;7:3540. [PubMed: 17960947]
13. Ginzburg VV, Balijepailli S. Nano Letters 2007;7:3716. [PubMed: 17983249]
14. Jang SS, Goddard WA. Journal of Physical Chemistry C 2007;111:2759.
15. Qiao R, Roberts AP, Mount AS, Klaine SJ, Ke PC. Nano Letters 2007;7:614. [PubMed: 17316055]
16. Hu Y, Litwin T, Nagaraja AR, Kwong B, Katz J, Watson N, Irvine DJ. Nano Letters 2007;7:3056. [PubMed: 17887715]
17. Tully DC, Frechet JMJ. Chemical Communications 2001:1229.
18. Stasko NA, Johnson CB, Schoenfisch MH, Johnson TA, Holmuhamedov EL. Biomacromolecules 2007;8:3853. [PubMed: 18004811]
19. Naylor AM, Goddard WA, Kiefer GE, Tomalia DA. Journal of the American Chemical Society 1989;111:2339.
20. Tomalia DA, Naylor AM, Goddard WA. Angewandte Chemie-International Edition in English 1990;29:138.
21. Hong SP, Bielinska AU, Mecke A, Keszler B, Beals JL, Shi XY, Balogh L, Orr BG, Baker JR, Holl MMB. Bioconjugate Chemistry 2004;15:774. [PubMed: 15264864]
22. Mecke A, Majoros IJ, Patri AK, Baker JR, Holl MMB, Orr BG. Langmuir 2005;21:10348. [PubMed: 16262291]
23. Mecke A, Uppuluri S, Sassanella TM, Lee DK, Ramamoorthy A, Baker JR, Orr BG, Holl MMB. Chemistry and Physics of Lipids 2004;132:3. [PubMed: 15530443]
24. Lee H, Larson RG. Journal of Physical Chemistry B 2006;110:18204.
25. Lee H, Larson RG. Journal of Physical Chemistry B 2008;112:7778.
26. Hong SP, Leroueil PR, Janus EK, Peters JL, Kober MM, Islam MT, Orr BG, Baker JR, Holl MMB. Bioconjugate Chemistry 2006;17:728. [PubMed: 16704211]
27. Lindahl E, Hess B, van der Spoel D. Journal of Molecular Modeling 2001;7:306.
28. Marrink SJ, Risselada HJ, Yefimov S, Tieleman DP, de Vries AH. Journal of Physical Chemistry B 2007;111:7812.
29. Monticelli L, Kandasamy SK, Periole X, Larson RG, Tieleman DP, Marrink SJ. Journal of Chemical Theory and Computation 2008;4:819.
30. Marrink SJ, de Vries AH, Mark AE. Journal of Physical Chemistry B 2004;108:750.
31. Essmann U, Perera L, Berkowitz ML, Darden T, Lee H, Pedersen LG. Journal of Chemical Physics 1995;103:8577.
32. Berendsen HJC, Postma JPM, Vangunsteren WF, Dinola A, Haak JR. Journal of Chemical Physics 1984;81:3684.
33. Guex N, Peitsch MC. Electrophoresis 1997;18:2714. [PubMed: 9504803]
34. Brant DA, Flory PJ. Journal of the American Chemical Society 1965;87:2788.
35. Doi, M.; Edwards, SF. The theory of polymer dynamics. Clarendon Press; Oxford: 1986.
36. Theodorou DN, Suter UW. Macromolecules 1985;18:1206.
37. Lee H, Baker JR, Larson RG. Journal of Physical Chemistry B 2006;110:4014.
38. Humphrey W, Dalke A, Schulten K. Journal of Molecular Graphics 1996;14:33. [PubMed: 8744570]

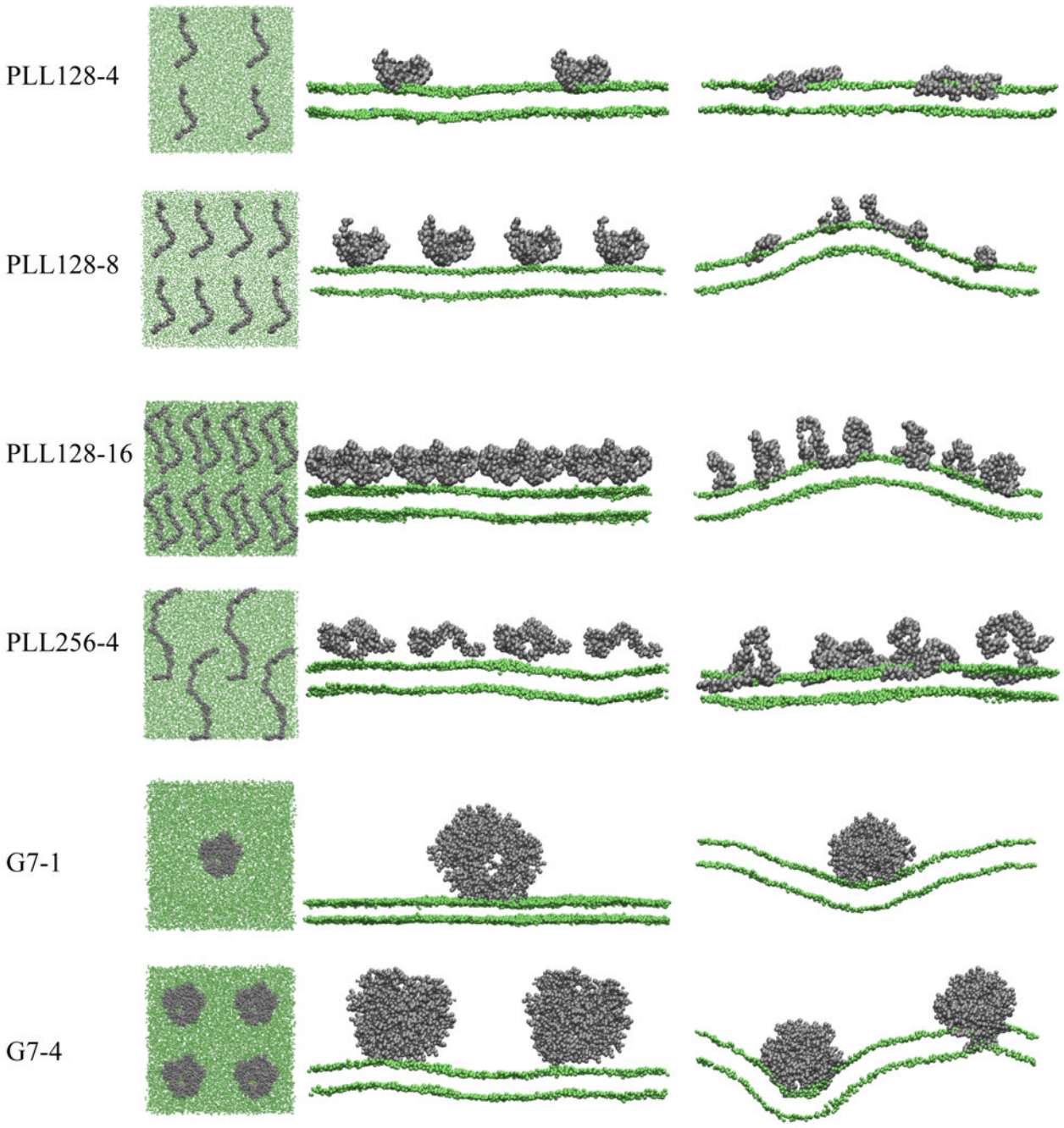

Figure 1.
Snapshots of the top view (*left image*) and side view (*middle image*) at the beginning (0 ns) and the side view at the end (200 ns for PLL, 240 ns for dendrimers, *right image*) of all simulations. Gray dots represent particles (PLL or dendrimers), and green dots represent headgroups of the DMPC bilayer. The explicit water, DMPC tails, and ions are omitted for clarity. Note that side views show only one cross section of the system and cannot capture all PLL or dendrimers. The images were created with VMD.[38]

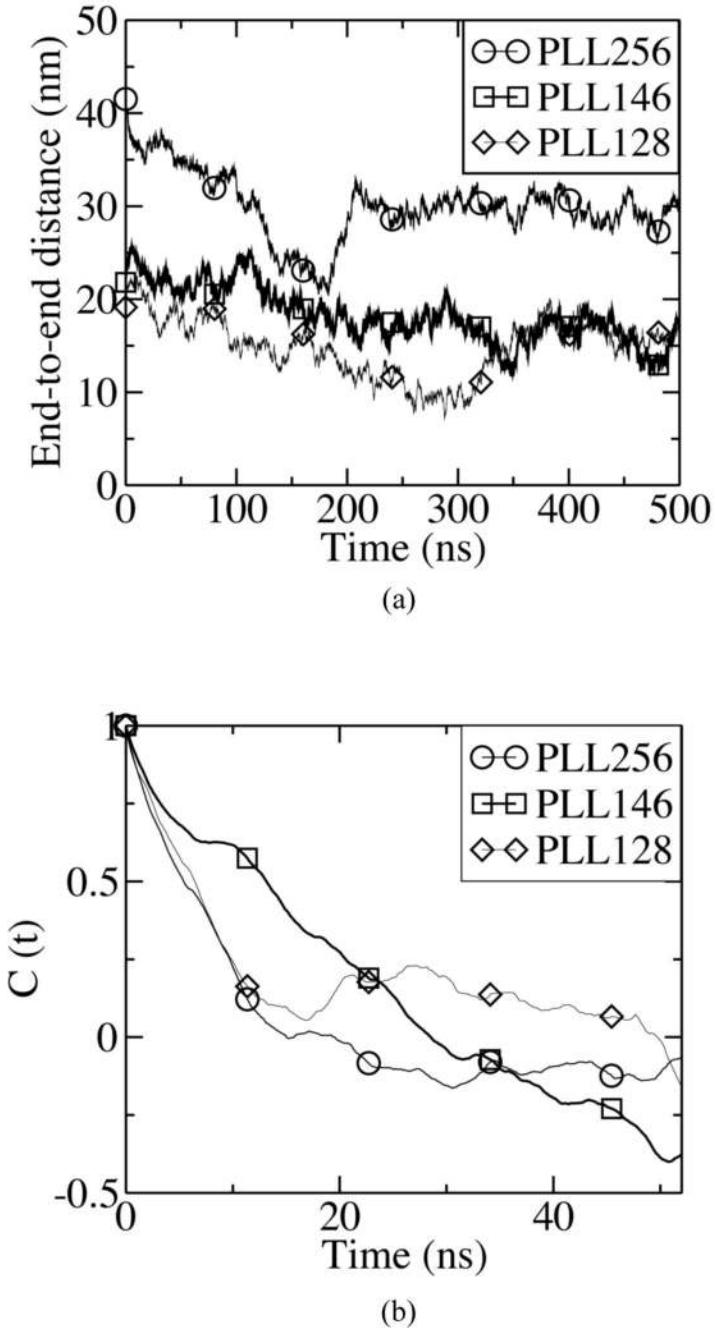

Figure 2.
(a) End-to-end distance and (b) its autocorrelation function (*C(t)*) for PLL128, PLL146, and PLL256, as functions of time.

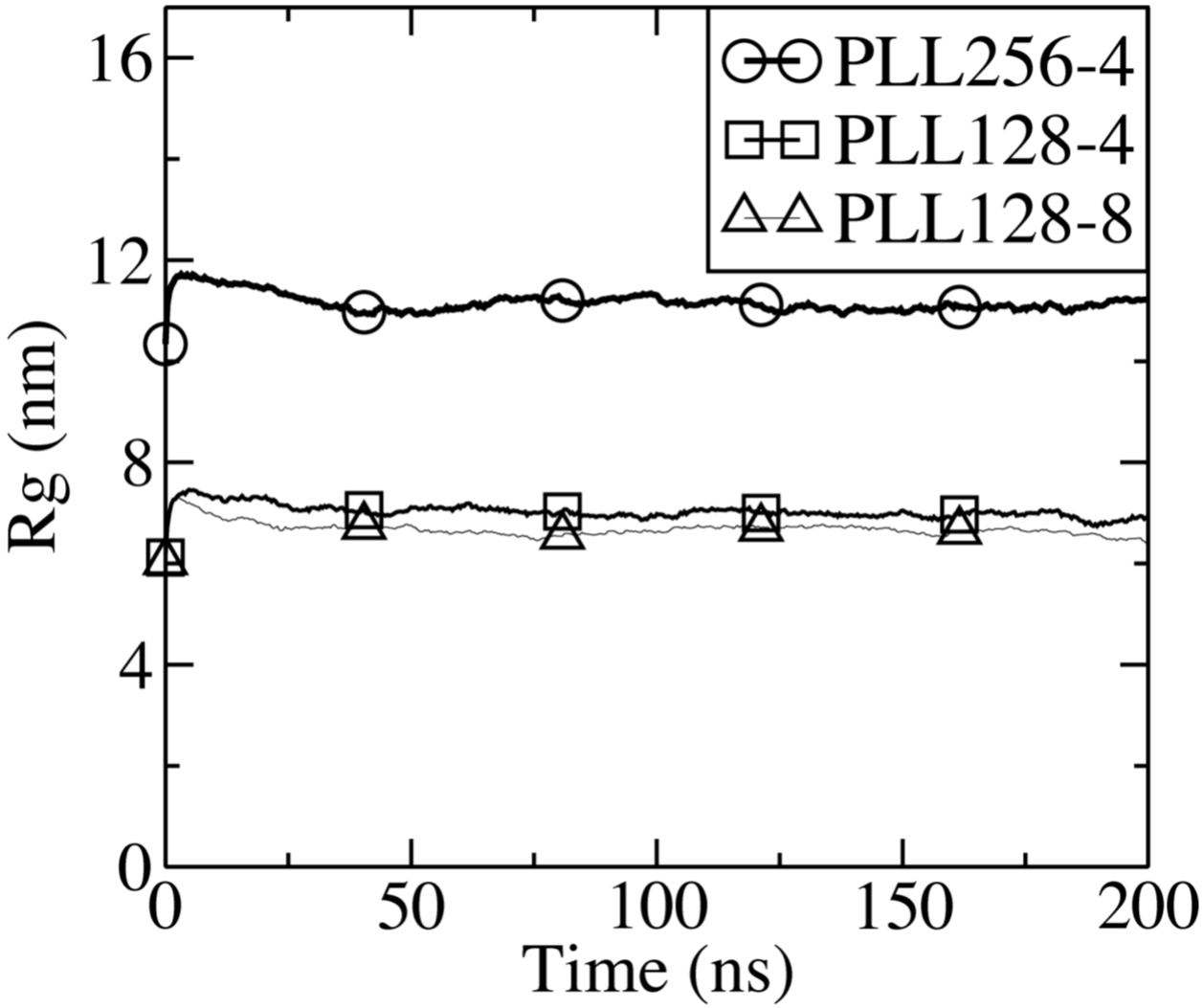

Figure 3.
Radii of gyration averaged over all PLL molecules of each PLL-bilayer simulation as a function of simulation time.

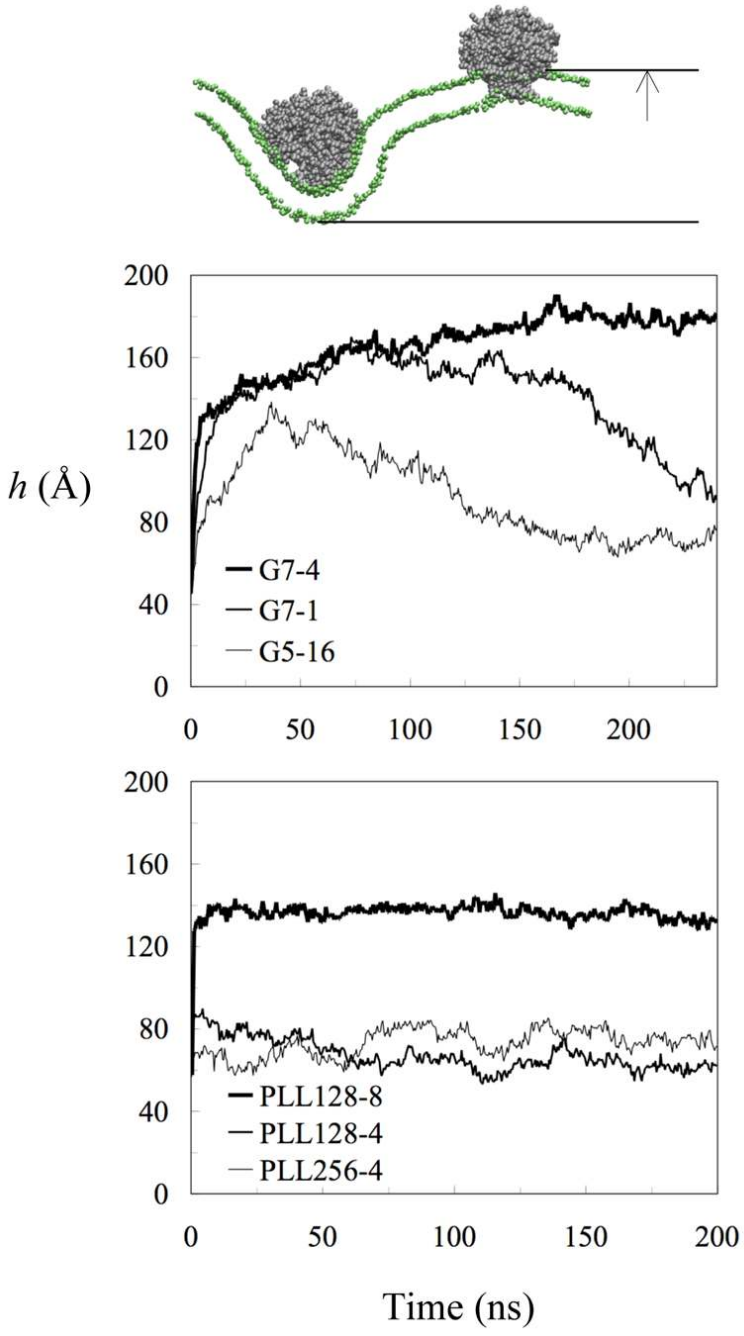

Figure 4.
Bilayer height, defined as the maximum distance between glycerols projected along the bilayer normal, as a function of time for the dendrimer-bilayer systems (top) and PLL-bilayer systems (bottom).

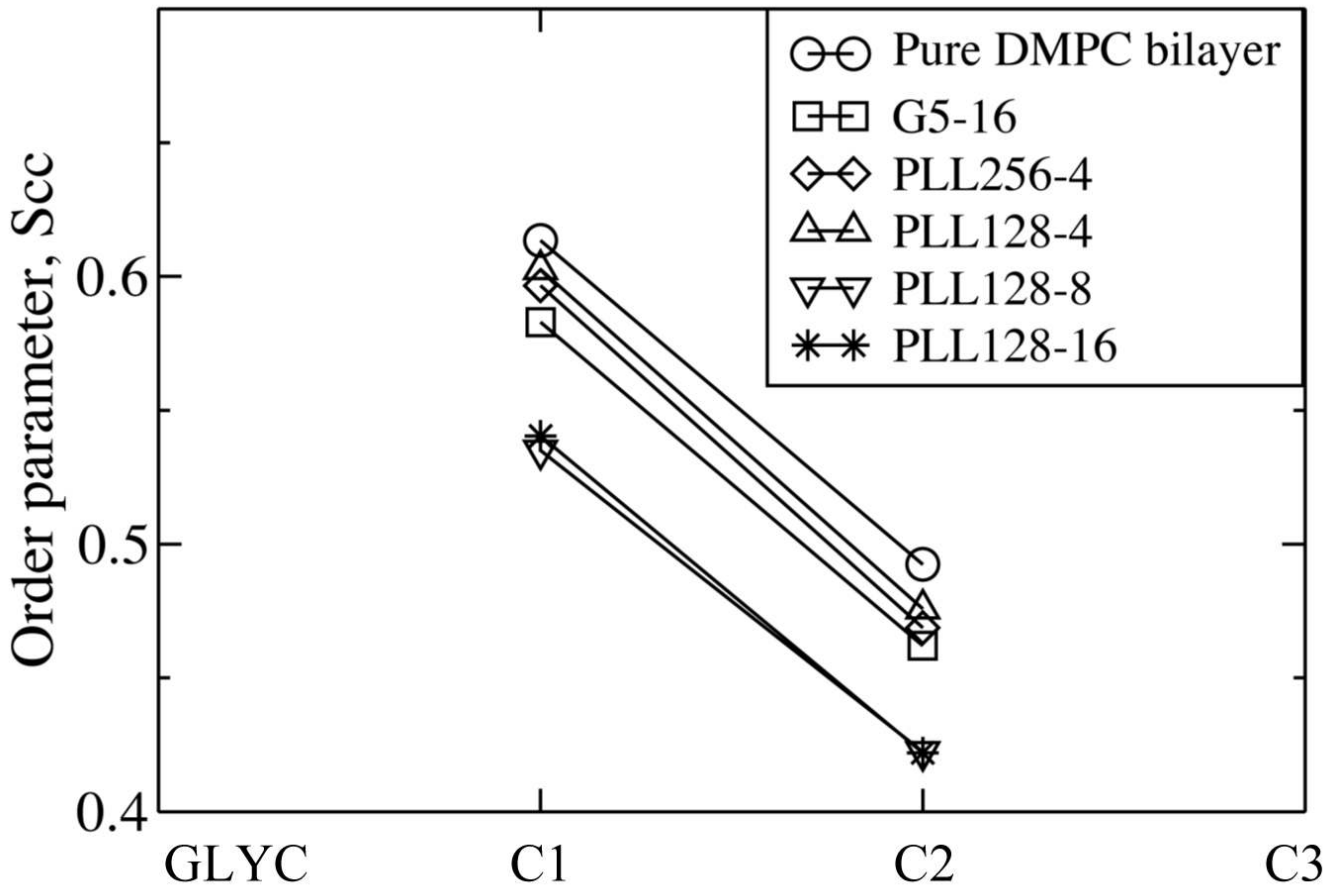

Figure 5.
Order parameters of DMPC tails in the pure bilayer, G5-16, PLL256-4, PLL128-4, PLL128-8, and PLL128-16, averaged over the last 40 ns. GLYC designates the bead for glycerol in DMPC, and C1 through C3 are beads for the tails.

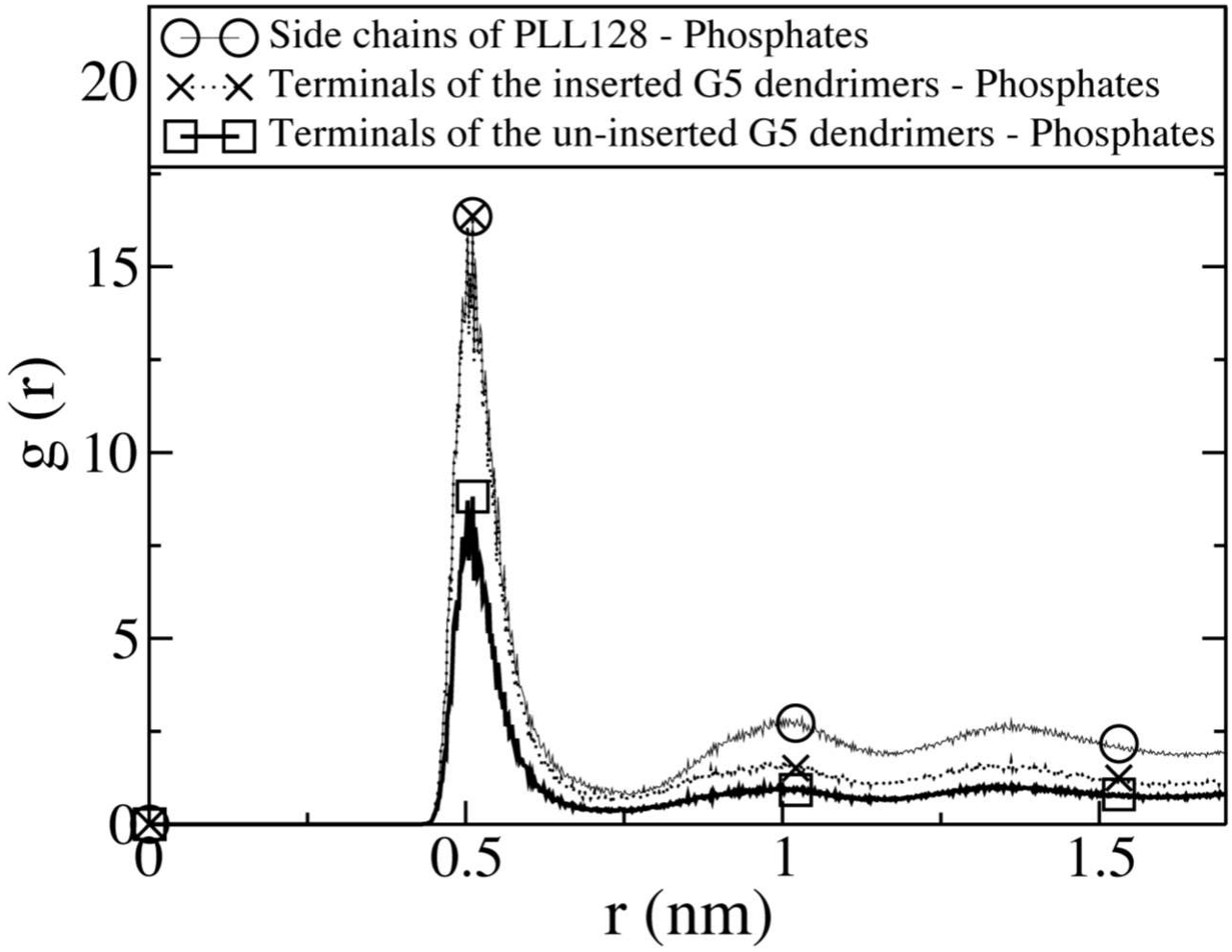

Figure 6.
Radial distribution functions of anionic DMPC phosphate groups with respect to the cationic side chain of PLL in PLL128-8, and the cationic terminals of dendrimers inserted or un-inserted into the bilayer in G5-16, averaged over the last 40 ns.

Table 1

List of simulations.

		PLL or dendrimer		No. of DMPC molecules	Simulation time (ns)
		No. of e^+ charges per molecule	No. of polymers		
Poly-L-Lysine (Linear, flexible)	PLL128-4	128	4	8192	200
	PLL128-8	128	8	8192	200
	PLL128-16	128	16	8192	200
	PLL256-4	256	4	8192	200
Dendrimer (Spheroidal)	G5-16*	128	16	8192	240
	G7-1*	512	1	8192	240
	G7-4*	512	4	8192	240

*These simulations were extended from the end (160 ns) of previous simulations.[25]

J Phys Chem B. Author manuscript; available in PMC 2009 March 17.

Table 2

Root-mean-square end-to-end distance ($\sqrt{\langle R^2 \rangle_0}$), averaged over the last 180 ns.

	$\sqrt{\langle R^2 \rangle_0}$ (Å)	
	Simulation	**Experiment**[34]
PLL128	162 ± 49	154 ± 15
PLL146	159 ± 53	166 ± 17
PLL256	296 ± 47	226 ± 23

Table 3

Average values of the principal moments of inertia, aspect ratios, and relative anisotropies of each PLL molecule for PLL128 and PLL256 over the last 180 ns, and for PLL128-4, PLL128-8, and PLL256-4 over the last 40 ns.

	Molecule	Principal moments of inertia (a.m.u. 10^3 nm^2)			Aspect ratio		Relative shape anisotropy
		I_z	I_y	I_x	I_z / I_y	I_z / I_x	
PLL128		946 ± 28	870 ± 19	129 ± 7	1.1	7.3	0.16
PLL128-4 (No bilayer curvature)	1	1016 ± 10	915 ± 10	108 ± 2	1.1	9.4	0.18
	2	638 ± 10	510 ± 14	139 ± 4	1.3	4.6	0.12
	3	685 ± 308	390 ± 7	301 ± 408	1.8	2.3	0.06
	4	853 ± 27	719 ± 17	142 ± 5	1.2	6.0	0.15
PLL128-8 (Bilayer curvature)	1	759 ± 7	696 ± 9	72 ± 6	1.1	10.6	0.19
	2	632 ± 67	543 ± 39	100 ± 3	1.2	6.3	0.15
	3	836 ± 5	809 ± 8	41 ± 5	1.0	20.1	0.21
	4	470 ± 8	453 ± 8	61 ± 4	1.0	7.7	0.17
	5	1043 ± 43	1012 ± 56	48 ± 4	1.0	21.5	0.22
	6	485 ± 76	380 ± 148	137 ± 3	1.3	3.5	0.10
	7	859 ± 49	806 ± 122	63 ± 13	1.1	13.6	0.20
	8	745 ± 82	719 ± 69	64 ± 10	1.0	11.3	0.19
PLL256		2839 ± 227	2792 ± 206	196 ± 46	1.0	14.5	0.20
PLL256-4 (No bilayer curvature)	1	4557 ± 29	4406 ± 42	307 ± 5	1.0	14.8	0.20
	2	3529 ± 69	3376 ± 106	304 ± 12	1.0	11.6	0.19
	3	4080 ± 926	3789 ± 323	341 ± 5	1.1	12.0	0.19
	4	3850 ± 53	3756 ± 56	322 ± 20	1.0	11.9	0.19